Chinese Chemical Letters 37 (2026) 111388

Contents lists available at ScienceDirect

Chinese Chemical Letters

journal homepage: www.elsevier.com/locate/cclet

Regulation of bound water molecular state in mineral-based electrolyte for highly stable aqueous Zn-MnO_2 batteries

Jing Huang[a], Zhexuan Liu[b,*], Hailong Li[c], Xiaoyu Wu[c], Kun Liu[a,*], Shuquan Liang[c], Guozhao Fang[c,*]

[a] School of Minerals Processing and Bioengineering, Central South University, Changsha 410083, China
[b] College of Chemistry and Chemical Engineering, Central South University of Forestry & Technology, Changsha 410004, China
[c] School of Materials Science and Engineering, Central South University, Changsha 410083, China

ARTICLE INFO

Article history:
Received 2 April 2025
Revised 25 May 2025
Accepted 28 May 2025
Available online 28 May 2025

Keywords:
Kaolin
Electrolyte regulation
Water molecule state
Charge carrier transport
Aqueous zinc-manganese batteries

ABSTRACT

The instability of the Zn metal anode in aqueous zinc-ion batteries is the main culprit limiting promotion and practicability. Solid-liquid hybrid electrolytes, as an emerging system containing electrochemically inert fillers, have been proposed and shown significant progress in recent years. The electrolyte regulation for suppressing side reactions mainly depends on the state of bound water molecules, so exploring the influence of intrinsic properties of fillers on electrolyte structure is of great significance. This work compared the effects of kaolin and its derived mullite on the state of bound water molecules and electrochemical behaviors in hybrid electrolytes. Relying solely on the high specific surface area of mullite is not sufficient to provide enough ion diffusion paths and limit water molecule activity, resulting in severe polarization and side reactions. The layered structure of kaolin can accommodate a large number of water molecules, which constructs hydrogen bonding networks for H^+ transport as the charge carrier with lower energy barrier. Hence, the kaolin-based electrolytes can inherit both low polarization of conventional liquid electrolytes and the durability to side reactions of hybrid electrolytes simultaneously. As a result, the aqueous Zn-MnO_2 battery with kaolin-based electrolyte can provide high specific capacity of ~300 mAh/g at 100 mA/g, and maintain at least 164 and 85.2 mAh/g at 300 and 500 mA/g for >500 cycles.

© 2026 Published by Elsevier B.V. on behalf of Chinese Chemical Society and Institute of Materia Medica, Chinese Academy of Medical Sciences.

Benefitting from the high energy density (5.85 Ah/cm^3) and relatively low potential (−0.76 V *vs.* SHE) of Zn metal, the safe, environmentally friendly and non-toxic aqueous zinc metal batteries are highly valued in the field of large-scale energy storage [1–4]. However, under the adsorption and dissociation of highly active water molecules at the interface, zinc metal anode is not resistant to conventional aqueous electrolytes and will be severely corroded to form ZSH passivation [5–8]. Meanwhile, the energy storage reaction of cathode materials in aqueous environments usually involves the H^+ intercalation and the cathode dissolution, leading to fluctuations in electrolyte pH and accelerating the zinc metal anode side reactions [9–11]. This greatly suppresses the long-life cycle stability and is also a major obstacle to the further practical application of zinc metal batteries.

Essentially, the stability of zinc metal anode largely depends on the regulation of water molecule states [12–16]. In recent years, the introduction of electrochemically inert fillers and the proposal of solid-liquid hybrid electrolytes have improved the long-life cycle stability of zinc metal batteries significantly [17]. However, given the diversity of electrochemical inert fillers, mainly the clay minerals, there has been no differential understanding of the distribution and state of bound water molecules in hybrid electrolytes. The differences in crystal structure of clay minerals affect the adsorption sites of water molecules, which in turn determine their reactivity towards proton conduction, charge transfer and ion diffusion [18]. For instance, the montmorillonite with adjustable interlayered structure could achieve species intercalation and ion exchange [19–21]. The properties of interlayered species not only change the interlayer spacing and ion diffusion path size, but their hydrophilicity also determines the state of bound water molecules [22–24]. Compared to the efficient utilization of interactions between lattice gaps and species, the minerals with anion close-packed lattice frameworks, including perovskite and silicon oxide [25,26], mainly rely on surface properties [27]. The dangling bonds at the mineral surfaces can attract a large number of ions and water molecules, constructing diffusion paths with relatively low

* Corresponding authors.
E-mail addresses: lzxuan@csuft.edu.cn (Z. Liu), kliu@csu.edu.cn (K. Liu), fg_zhao@csu.edu.cn (G. Fang).

https://doi.org/10.1016/j.cclet.2025.111388
1001-8417/© 2026 Published by Elsevier B.V. on behalf of Chinese Chemical Society and Institute of Materia Medica, Chinese Academy of Medical Sciences.

coordination numbers and high Gibbs free energy for interfacial ion conduction [28]. Although different clay minerals can inhibit water molecule activity to varying degrees, excessive binding is not conducive to electrode interfacial reaction kinetics and weak adsorption is also difficult to suppress side reactions completely. The relationship between crystal structure differences of clay minerals, the state of bound water molecules in hybrid electrolytes, and the electrochemical behavior and performances have not been studied.

Here, in order to fully reveal the influence of bound water molecule state on electrochemical performances in hybrid electrolytes, this work compared kaolin with layered structure (KLCP) and its derivative mullite with anion close-packed after calcination (CKL) systematically. The unavailable charge carrier transport, which is caused by firm adsorption of Zn^{2+} by CKL surface, results in a high diffusion energy barrier and sluggish reaction kinetics. The limited CKL surface is also difficult to bind all water molecules and suppress side reactions, resulting in uneven deposition of zinc anode and irreversible lattice collapse of manganese-based cathode. In contrast, the KLCP can accommodate intercalated water molecules at the interlayered space and limit their high activity through layer-to-layer van der Waals forces. More importantly, the interlayer binding of water molecules forms abundant hydrogen bonding network for H^+ transport, while achieving suppressed water molecule activity and rapid charge carrier transport kinetics simultaneously. Hence, the Zn-δ-MnO_2 batteries in KLCP-ZMSO electrolyte could maintain specific capacity of 164 mAh/g at 500 mA/g for 500 cycles, while the specific capacity in CKL-ZMSO suffers from declined stability and lower electrochemical activity of 85.2 mAh/g. By researching the influence of clay mineral lattice structure on electrolyte performances, novel methods and scientific guidance can be provided for further electrolyte rational design.

The XRD pattern shows the difference between pure kaolin (KLCP) and calcined kaolin (CKL) (Fig. 1a). The KLCP diffraction pattern fully reflects the diffraction characteristics of Kaolin-1A phase (PDF #14–0164), with the two strongest diffraction peaks at $2\theta = 12.3°$ and 24.8° corresponding to the (001) and (002) crystal planes, respectively. CKL is formed by high-temperature calcination of ordinary kaolin above 1000 °C. Its diffraction pattern mainly shows mullite phase (PDF #15–0776) and contains characteristic peaks of quartz phase (PDF #39–1425) [29]. As an aluminosilicate mineral with layered structure, KLCP consists of ordered stacking of silicon oxide layers composed of [SiO_4] tetrahedra and aluminum oxide layers composed of [AlO_6]-(OH) octahedra (Fig. 1b).

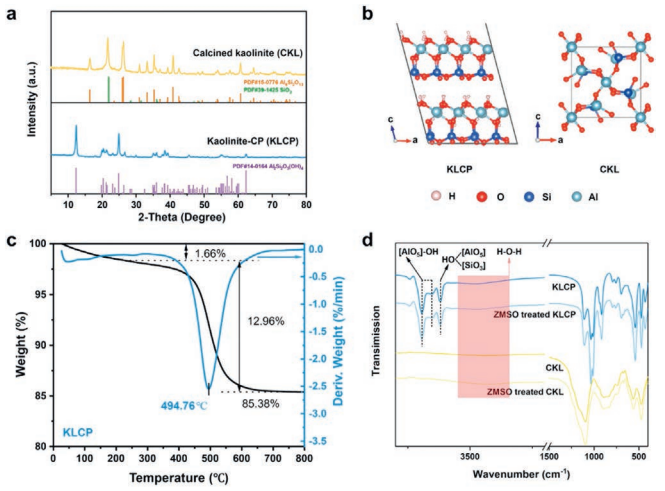


Fig. 1. Differences in crystal structure and adsorption of water molecule. (a) XRD patterns and (b) crystal structures of KLCP and CKL. (c) TG curves of KLCP. (d) FT-IR of pristine and ZMSO electrolyte treated KLCP and CKL.

The van der Waals binding force between the layers is weak and carries inherent negative charges, making it easy to form materials with larger specific surface area and better adsorption capacity for cations. In the electrolyte system of zinc ion batteries, it can serve as an ion storage and transport channel, providing uniformly distributed reaction sites. In contrast, the lattice framework of mullite is composed of the edge-to-edge connections between [AlO_6] octahedra and corner-to-corner connections between [AlO_6] octahedra and [SiO_4] tetrahedra. According to the difference in the elemental ratio of Si and Al, there are differences in the lattice parameters. The mullite does not provide obvious channels for ion diffusion, which leads to its interface properties dominating the ion transport behaviors.

Due to differences in crystal structure, the kaolin and its derived mullite exhibit significant differences in the adsorption of molecules or ions. As previously reported, CKL relies on surface hydrogen bond interactions merely to adsorb water molecules, and the weak binding makes it difficult for water molecules to be retained. As a result, the TG curve of CKL shows only ~1 wt% weight loss even heating to 800 °C (Fig. 1c). The interlayer space of KLCP can accommodate abundant water molecules (~15 wt%), which can only be removed completely at 500 °C (Fig. S1 in Supporting information), indicating strong binding between interlayer water molecules and the lattice framework [30]. The difference in water content between KLCP and CKL can also be proved by FT-IR [31,32]. As shown in Fig. 1d, no obvious band of O–H bond in water molecules could be observed in CKL, and the bands did not change significantly after ZMSO electrolyte immersion treatment. This indicates that CKL cannot provide sufficient lattice gaps to accommodate water molecules, thereby failing to limit water molecule activity and promote H^+ transport effectively. In contrast, except for the O–H band from water molecules, more bands can be observed at 3693/3650 and 3620 cm^{-1} in KLCP, which can be attributed to the O–H stretching outside the [AlO_6] octahedron, and the O–H stretching on the binding surface between the [SiO_4] tetrahedron/[AlO_6] octahedron, respectively. This indicates that KLCP lattice can accommodate more water molecules and achieve strong binding of water molecules with abundant hydroxyl groups.

Given the difference in the state of bound water molecules in silica-alumina oxides minerals, the activity difference of water molecules will directly determine their electrochemical behaviors. Typically, the absence of mineral adsorption in conventional aqueous electrolyte ZMSO to reduce the activity of free water molecules results in the highest corrosion current of 2.223 mA/cm^2 (Fig. 2a). The CKL can limit the activity of water molecules, suppress zinc corrosion and reduce corrosion current to some extent due to its high specific surface area and interfacial hydrogen bonding. More importantly, the KLCP can not only adsorb water molecules, but its layered structure can also further suppress the side reactions caused by water molecules, thereby achieving the lowest corrosion current of 0.977 mA/cm^2. Similar phenomenon could also be observed from the LSV curves, in which the KLCP-ZMSO hybrid electrolyte exhibits higher electrochemical stability (Fig. 2b). Due to the limited specific surface area, most of the water molecules in the CKL-ZMSO electrolyte are not adsorbed on the surface of CKL, and a large number of free water molecules result in the narrow electrochemical stability window (0.715 V) similar to that of ZMSO electrolytes (0.705 V). For KLCP, its layered structure ensures that most water molecules are intercalated between layers or adsorbed on the surface, which makes it difficult to be electrolyzed and produce gas.

The state of the bound water molecule not only determines its induced side reactions, but also the transport of charge carriers in the electrolyte. As shown in Fig. 2c, the number of ion migrations in the electrolyte is tested and calculated. The conventional liquid

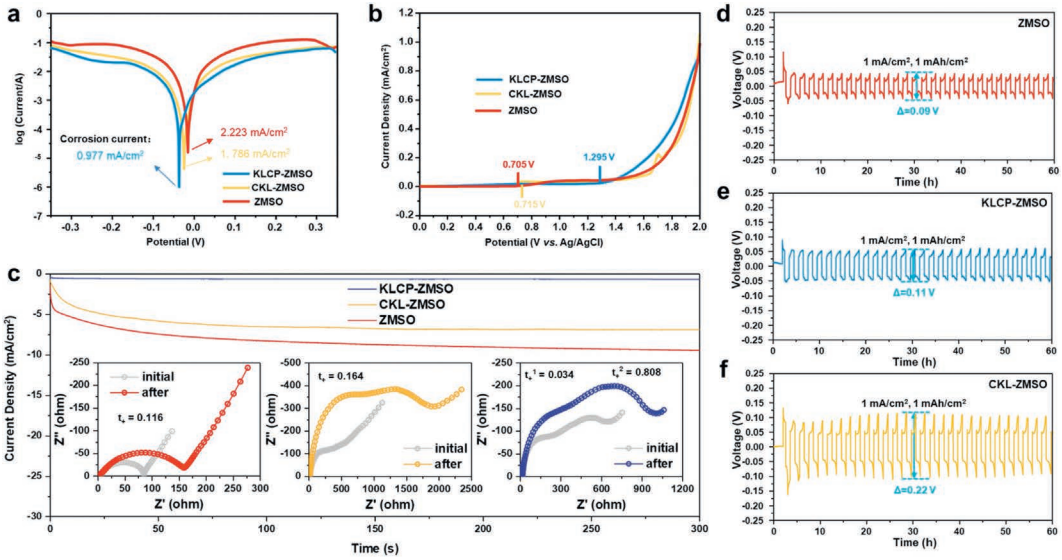


Fig. 2. Electrochemical behavior induced by difference of water state. (a) Tafel, (b) LSV curves and (c) calculated ion transfer number in different electrolytes. Zn/Zn symmetric cell cycle polarization under 1 mA/cm^2@1 mAh/cm^2 in (d) ZMSO, (e) KLCP-ZMSO and (f) CKL-ZMSO electrolytes.

electrolyte ZMSO exhibits a standard impedance response with an ion transfer number t_+ of 0.116, which is common in conventional liquid electrolytes because the anions are significantly involved in diffusion and reaction, especially the OH^- in aqueous environment. The CKL-ZMSO also exhibits only one impedance response in the initial state, which indicates the abundant free water molecules [33]. However, two impedance responses could be observed after *CA*, representing the interfacial charge transfer impedance and the ion diffusion impedance at the interface of particles in hybrid electrolyte. Since the water molecules in the CKL-ZMSO are mainly adsorbed on the surface of CKL and in contact with the zinc anode surface directly, the calculated ion transfer number according to the interfacial Zn^{2+}/Zn charge transfer is similar to that of ZMSO (0.164). The ion transfer number of Zn^{2+}/Zn plating/stripping interfacial charge transfer in KLCP-ZMSO is 0.034, which is understandable because the layered structure of KLCP accommodates most of the water molecules at the interlayers, and thus results in the lack of sufficient water molecules to facilitate Zn^{2+}/Zn plating/stripping. However, it should be noted that the calculated ion transfer number according to the ion diffusion impedance reached 0.808, indicating the dominant role of cation transfer in bulk hybrid electrolyte. Considering that the ion transfer number of the interfacial process is much lower than that of bulk process, the ions transported in bulk may not be limited to Zn^{2+} from the interface. Hence, it is reasonable to infer that the binding of water molecules in the layered KLCP makes it more inclined to dissociate into H^+ and OH^-. The stripped Zn^{2+} mainly accumulates at the zinc anode interface and combines with OH^- and SO_4^{2-} to form $Zn_4SO_4(OH)_6{\cdot}nH_2O$ (ZSH), while the remaining H^+ is transferred in electrolyte bulk as the charge carrier.

Hence, the effects of electrolytes on the cycling performance of Zn/Zn symmetric batteries were studied under the conditions of 1 mA/cm^2@1 mAh/cm^2. As shown in Fig. 2d, due to the complete solvation effect to reduce the electrostatic repulsion suffered by ion conduction, as well as the low viscosity of conventional aqueous solutions, the polarization in ZMSO is only 0.09 V [34]. Although the Zn^{2+} diffusion in KLCP is not as fast as ZMSO, the adsorbs abundant water molecules stimulates the diffusion of H^+ with lower ionic radius and weaker electrostatic repulsion at the interlayer space. On the one hand, the interlayered species can significantly broaden the lattice parameters of KLCP along the (001) orientation, accommodating more water molecules and providing wider ion diffusion paths for both Zn^{2+} and H^+. On the other hand, abundant interlayered water molecules adsorb on $[SiO_4]$/$[AlO_6]$ slabs to construct hydrogen bonding networks, paving the way for H^+ diffusion based on Grotthuss mechanism. As a result, the KLCP-ZMSO electrolyte exhibits the similar superior Zn^{2+}/H^+ conduction kinetics and polarization to conventional liquid ZMSO electrolyte (Fig. 2e). In sharp contrast, the Zn/Zn symmetric battery with CKL-ZMSO electrolyte exhibit significantly more serious polarization (Fig. 2f), indicating sluggish Zn^{2+} conduction kinetics in bulk electrolyte. This is mainly because the Zn^{2+} adsorbed on the CKL surface suffer from stronger electrostatic attraction and coordination, and these Zn^{2+} located in thermodynamically stable states are also more difficult to achieve interfacial diffusion. As a result, the sluggish ion diffusion kinetics in CKL-ZMSO cause severe polarization and Zn/Zn symmetric battery failure within 100 h, while uncontrolled dendrites in ZMSO can also lead to short circuits quickly despite weak polarization (Fig. S2 in Supporting information). In contrast, the charge carrier transport mechanism in KLCP-ZMSO, which is not limited to Zn^{2+}, achieves a good balance between kinetics and stability, without obvious degradation after cycle for >400 h. Meanwhile, the Cu/Zn asymmetric batteries in KLCP-ZMSO also exhibit moderate polarization and the most stable high Coulombic efficiency (Fig. S3 in Supporting information), which is consistent with the polarization in Zn/Zn symmetric batteries.

DFT calculations were carried out to further demonstrate the interactions between CKL or KLCP with molecules/ions in electrolyte. As shown in Fig. 3a, the adsorbed water molecules could participate in the coordination environment of the interfacial Al/Si atoms at the CKL surface, and the formed Si/Al-OH_2 bonds tightly to confine the water molecules. Due to the binding water molecules and hydroxyl groups at the KLCP interlayers, the accommodated water molecules form abundant hydrogen bonding interactions with water molecules or hydroxyl groups. Such hydrogen bonding interaction endows water molecules higher degrees of freedom and lower polarization, which can promote more frequent proton hopping and faster diffusion kinetics between water molecule. Moreover, as shown in Fig. 3b, KLCP not only exhibits higher adsorption energy with water molecules (-0.43 eV > -0.82 eV for CKL), but also the weaker adsorption

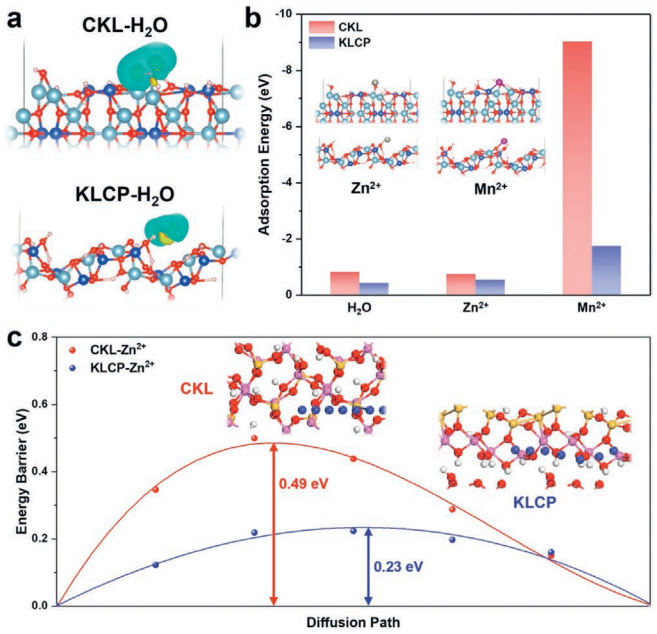


Fig. 3. Calculated kinetics behavior of molecules and ions in CKL and KLCP. (a) Differential charge density of H_2O molecule adsorption at the interface of CKL and KLCP. (b) Adsorption energy of water molecule, Zn^{2+} and Mn^{2+} on CKL and KLCP. (c) Diffusion energy barrier of Zn^{2+} in CKL and KLCP.

with Zn^{2+}/Mn^{2+} (-0.54 eV $>$ -0.74 eV for Zn^{2+}, and -1.74 eV $>$ -9.02 eV for Mn^{2+}) lays the foundation for the rapid conduction kinetics. More specifically, according to the calculated diffusion energy barriers of Zn^{2+} in CKL and KLCP (Fig. 3c), it can be observed that the Zn^{2+} diffusion faces a maximum energy barrier of 0.49 eV when it diffuses into the lattice gaps lacking coordination atoms in CKL. Throughout the Zn^{2+} diffusion process in KLCP, abundant water molecules or hydroxyl groups participate in its coordination structure. The insignificant fluctuations in the coordination environment promote relative stability of energy change, resulting in a diffusion energy barrier of only 0.23 eV ultimately.

Manganese-based cathode materials has been widely studied due to its high capacity and high operating voltage [35,36]. Among them, δ-MnO_2 has a layered structure, and the large interlayer spacing provides an ideal storage and Zn^{2+} transport paths. Hence, we compared the performance of different cathode materials, including layered structure δ-MnO_2 and F doped δ-MnO_2 (named δ-MnO_2-F), to further analyze the effect of bound water molecule state in electrolyte on the electrodes. From Fig. 4a, it can be seen that the specific capacity of the battery exhibits a clear size relationship of KLCP-ZMSO > ZMSO > CKL-ZMSO at a current density of 100 mA/g, with the former being about 27 % and 34 % higher than the latter two, respectively. At the same time, KLCP-ZMSO electrolyte effectively improves the cycling stability of zinc manganese batteries, with almost no capacity degradation after 100 cycles. Similarly, at a current density of 200 mA/g, the battery containing KLCP-ZMSO exhibited the highest specific capacity, and can stably cycle 350 times (Fig. S4 in Supporting information). It can be seen that the modification effect of pure kaolin KLCP is the best, due to its sheet-like structure's ion exchange and storage characteristics. During the charge and discharge process, it provides the reaction active sites at the cathode and anode surface, controlling the diffusion and deposition behavior of Mn^{2+} and Zn^{2+}. In the KLCP-ZMSO electrolyte, Zn-δ-MnO_2 batteries also exhibited excellent cycling stability performance, showing specific capacities of approximately 164, 85.2 and 83.1 mAh/g after 500 cycles at current densities of 300, 500 and 1000 mA/g, respectively (Fig. 4b and Fig. S5 in Supporting information). In addition, the Zn-δ-MnO_2 batteries could recover to the specific capacity of 181.3 mAh/g under 0.2 C after cycling at high current densities of 1 C, exhibiting superior rate performance (Fig. 4c). In contrast, the sluggish reaction kinetics in CKL-ZMSO limit the electrochemical activity of manganese-based cathodes, and the obviously higher Coulombic efficiency under 0.2 C in ZMSO indicates the probable irreversible manganese deposition reaction though exhibiting higher specific capacity.

Except for the synthesized manganese-based cathode materials with special morphology and high electrochemical activity, the commercial electrolytic MnO_2 cathode, which has lower electrochemical activity, was also assembled with different electrolytes, further proving the practicability and availability. From Fig. S6 (Supporting information), it can be seen that at a current density of 100 mA/g, the battery with ZMSO electrolyte experienced severe capacity degradation, mainly due to changes such as dissolution and irreversible deposition caused by the inherent characteristics of MnO_2. The battery using KLCP-ZMSO electrolyte showed a significant improvement in cycling stability, with stable cycling for 300 cycles at a current density of 500 mA/g (Fig. 4d).

In order to investigate the excellent electrochemical performances in KLCP-ZMSO electrolyte, the detailed electrochemical characterization was conducted. As shown in Fig. S7a (Supporting information), CV curves were tested with different cycle numbers under the condition of a scanning speed of 0.1 mV/s. In KLCP-ZMSO electrolyte, the battery still exhibits similar redox peaks to conventional zinc-manganese batteries, indicating that the addition of KLCP does not change the reaction mechanism. The KLCP only has a significant effect on reducing the activity of water molecules and suppressing side reactions. Moreover, the highly overlapping CV curves indicates that the KLCP-ZMSO electrolyte promotes satisfactory interfacial compatibility and cycle stability. Based on the CV curves under different scanning rates, as shown in Fig. S7b (Supporting information), the current increase as the scan rate increases from 0.1, 0.2, 0.4, 0.6, 0.8 mV/s to 1 mV/s, while the increase magnitude of the current is relatively low. This indicates that the proportion of pseudocapacitive behavior during electrode reactions is relatively low in KLCP-ZMSO electrolyte. This phenomenon can be explained by the low ion diffusion rate in the mixed electrolyte [37]. Although the addition of KLCP reduces the activity of water molecules and improves the cycling stability of the battery effectively, it also sacrifices the ion conductivity in the aqueous electrolyte to some extent, thus partially suppressing the capacitance behavior of the battery. In addition, it could also be observed that the potential of the peaks shifted significantly, which further indicates that the KLCP will reduce the ion conductivity, resulting in higher polarization compared to conventional liquid electrolytes.

The detailed explanation of the specific control process of the electrode reaction was demonstrated by calculating the electrode reaction pseudocapacitance behaviors. Here, the oxidation–reduction peaks of the charging and first discharge platforms were selected for analysis (the charging peak is labeled as Peak 1, and the first discharge peak is labeled as Peak 2) (Figs. S7c and d in Supporting information). Firstly, the peak current corresponding to each scanning speed was selected, and then the logarithm of the peak current and scanning speed was calculated. Then, a linear fitting was performed on the calculated peak current and the logarithm of the scanning speed. The slope of its linear fitting is denoted as b value, which can indicate whether the battery reaction is controlled by diffusion or pseudocapacitance. Generally speaking, the magnitude of b value ranges from 0.5 to 1. When b value approaches 0.5, the electrode reaction is mainly controlled by diffusion process; When the value of b approaches 1, it is mainly controlled by pseudocapacitance. According to the calculation results of b-value, $b_{Peak\ 1} = 0.52$ and $b_{Peak\ 2} = 0.50$, both b-values are close to 0.5, indicating that the electrode reaction in KLCP-ZMSO

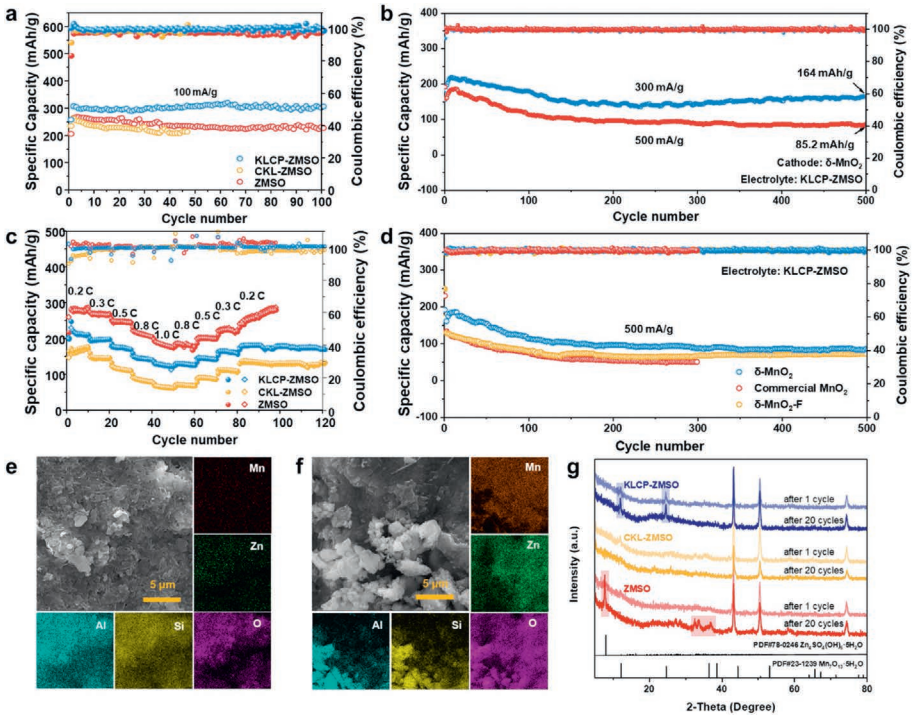


Fig. 4. Electrochemical performances and morphology evolution of manganese-based cathode. (a) Cycle performances of δ-MnO_2 in ZMSO, CKL-ZMSO and KLCP-ZMSO at 100 mA/g. (b) Cycle performances of δ-MnO_2 in KLCP-ZMSO at 300 and 500 mA/g. (c) Rate performances of δ-MnO_2 in ZMSO, CKL-ZMSO and KLCP-ZMSO (1 C = 1000 mAh/g). (d) Cycle performances of different cathodes in KLCP-ZMSO at 500 mA/g. SEM images and EDS mapping of cathode at charged states after 10 cycles in (e) KLCP-ZMSO and (f) CKL-ZMSO electrolytes. (g) XRD patterns of cathode at charged states after cycles in different electrolytes.

electrolyte is mainly controlled by diffusion process. In summary, KLCP-ZMSO electrolyte does not affect the normal electrode reaction process of zinc manganese batteries. The KLCP can reduce the activity of water molecules and improve the cycling stability of the battery, but the ion conductivity of the electrolyte is reduced, making the electrode reaction mainly controlled by diffusion process.

LCP-ZMSO electrolyte not only improves cycling stability but also increases specific capacity. This can be analyzed by fitting the Mn 3s peak, as shown in Fig. S8 (Supporting information). The area ratio of Mn 3s to Zn 3p is CKL-ZMSO (6.09:1) < KLCP-ZMSO (6.73:1), and the distance between the two peaks of Mn 3s is CKL-ZMSO (4.9 eV) > KLCP-ZMSO (4.2 eV), indicating that the charged manganese valence state is CKL-ZMSO < KLCP-ZMSO, which suppresses the participation of Zn^{2+} in the reaction to form low electrochemical activity zinc manganese oxide in kaolin electrolyte. The main reaction is H^+, thereby generating products such as H_xMnO_2 or MnOOH and improving the specific capacity.

Herein, in order to quantitatively demonstrate the protective effect of kaolin-based electrolytes on manganese-based cathodes, further research was conducted on the self-discharge performance of batteries with ZMSO electrolyte and KLCP-ZMSO electrolyte. As shown in Fig. S9 (Supporting information), the curves of voltage over time and the changes in battery capacity under different electrolytes are presented, in which the battery stands for 24 h after two cycles. The voltage drop in KLCP-ZMSO electrolyte is 0.02 V smaller than that in ZMSO electrolyte, and higher capacity could be retained in KLCP-ZMSO (97.1 % > 94.7 % in ZMSO). A higher voltage maintenance means that there are fewer dissolution side reactions occurring in the electrolyte, and the electrode/electrolyte interface is more stable, ensuring the performance stability of the battery after long-term standing. Specifically, in the KLCP-ZMSO electrolyte system, the battery capacity after 24 h of standing still has 224.7 mAh/g, which is much higher than the 186.3 mAh/g in the ZMSO electrolyte system. In summary, the voltage and capacity of conventional liquid electrolyte systems decrease significantly over time, while batteries using KLCP-ZMSO electrolyte system exhibit better voltage and capacity retention over the same period of time. These data intuitively demonstrate that the addition of kaolin in the electrolyte not only improves the voltage retention ability of the battery, but also significantly enhances the capacity retention rate, which is beneficial for the long-term stability and cycle life of the battery.

The electrodes of ZMBs with KLCP-ZMSO and CKL-ZMSO electrolytes after cycling were characterized to confirm the affinity between kaolin and electrodes, as well as the effect of electrolytes on Zn^{2+} depositing/stripping during long-life cycle. Figs. 4e and f show the SEM images and EDS element distribution of cathodes in KLCP-ZMSO and CKL-ZMSO electrolytes, respectively. Compared to the distinct particle in CKL-ZMSO electrolyte, the cathode surface after cycling with KLCP-ZMSO electrolyte showed a smooth and intact positive electrode morphology. It can be seen that KLCP-ZMSO has good affinity with the δ-MnO_2 electrode, as manifested by the uniform coverage of Al and Si elements, which weakens the signal of Mn element. On the contrary, in CKL-ZMSO, it exhibits the characteristic of stacking and agglomeration, which is not conducive to the uniform reaction of Mn^{2+}. This optimized electrochemical process can also be confirmed by XRD. As shown in Fig. 4g, the δ-MnO_2 cathode dissolved after the first discharge in ZMSO electrolyte, and no obvious diffraction peaks could be observed after charging, indicating the low crystallinity of manganese oxide deposition. More importantly, the strong peaks of ZSH can still be detected on the surface of the charged cathode after 20 cycles, indicating irreversible ZSH accumulation and thus unfavorable reaction activity. The introduction of CKL adsorption to water molecules can suppress related side reactions, while the strong adsorption of cations also inhibits their diffusion and reaction at the cathode interface. Only a small amount of $Mn_7O_{13}{\cdot}5H_2O$ with low crystallinity could be observed during manganese deposition, and the diffraction peaks disappeared after 20 cycles. In contrast, the higher specific surface area and abundant ion diffusion paths

of KLCP promote the feasibility of interfacial manganese deposition/dissolution reactions. The Mn^{2+} dissolved during discharging can be intercalated and stored between the interlayers of KLCP, and then released reversibly during charging. The uniform adsorption of KLCP on the cathode surface also promotes the growth of $Mn_7O_{13}{\cdot}5H_2O$ nuclei, exhibiting the maintained diffraction peaks after 20 cycles.

Similarly, for Zn anode side, the CKL-ZMSO electrolyte clearly results in mineral particle aggregation and protrusion, while the surface of the Zn anode exhibits a "ripple-like" byproduct (Fig. S10a in Supporting information). The Zn anode after cycling with KLCP-ZMSO electrolyte exhibits a more uniform and flat surface morphology (Fig. S10b in Supporting information). In addition, the uniform distribution of Al and Si elements on the anode surface of KLCP-ZMSO electrolyte proves that kaolin particles are uniformly distributed on its surface. The distribution of Zn element in the surface of Zn anode is more uniform under the same charging state, indicating that the electrolyte plays a guiding role in the Zn^{2+} migration and platting/stripping behavior [38,39]. In other words, KLCP-ZMSO is a good adaptation electrolyte for Zn^{2+} in the electrochemical reaction process.

The electrochemically inert mineral fillers can regulate the state of bound water molecules in solid-liquid hybrid electrolytes based on their crystal structure differences, which is not just about adsorbing water molecules to reduce its derived side reactions. Specifically, the KLCP with wide interlayer spacing can not only promote water molecule adsorption top suppress side reactions, but also construct abundant hydrogen bonding networks as the conduction paths for H^+. The special charge carrier transport method with Grotthuss hopping mechanism and weaker electrostatic repulsion determines the low diffusion energy barrier, achieving both lower water molecule activity and faster ion diffusion kinetics. In contrast, the ions and molecules in CKL-ZMSO can only adsorb on the surface of mullite, especially for Zn^{2+}, suffering from limited diffusion kinetics due to the coordination with lattice oxygen on the mullite surface. Compared to the abundant lattice interlayered conduction in KLCP, the limited specific surface area of CKL is also difficult to suppress the activity of all water molecules, making it difficult to avoid side reactions.

In summary, this work investigated the influence of inorganic mineral fillers on the state of bound water molecules and electrochemical behavior in solid-liquid hybrid electrolytes. It can be concluded that the interaction between the surface and interlayer of kaolin and water molecules can not only achieve accommodation of abundant water molecules, but also provide ion diffusion paths constructed by hydrogen bonding networks between interlayered adsorbed water molecules. Hence, according to Tafel, LSV and symmetric Zn/Zn cell test results, the KLCP-ZMSO, with more water molecules than CKL-ZMSO, exhibited higher electrochemical stability. The abundant ion diffusion paths provided by interlayered KLCP also promote highly electrochemically active manganese oxide deposition, and uniform Zn platting/stripping and inhibit dendrite growth. As a result, the Zn-δ-MnO_2 batteries with KLCP-ZMSO electrolyte exhibited high specific capacity of $\sim$300 mAh/g at current densities of 100 mA/g, and maintained at least 164 and 85.2 mAh/g at 300 and 500 mA/g for at least 500 cycles. Meanwhile, the KLCP-ZMSO electrolyte is also suitable for commercial MnO_2 cathodes, demonstrating satisfactory practicality and providing insights for the future development of aqueous zinc-manganese battery systems.

CRediT authorship contribution statement

Jing Huang: Writing – original draft, Methodology, Conceptualization. **Zhexuan Liu:** Writing – review & editing, Supervision, Conceptualization. **Hailong Li:** Methodology. **Xiaoyu Wu:** Methodology. **Kun Liu:** Writing – review & editing, Supervision. **Shuquan Liang:** Writing – review & editing. **Guozhao Fang:** Writing – review & editing, Supervision, Resources, Funding acquisition.

Declaration of competing interest

The authors declare that they have no known competing financial interests or personal relationships that could have appeared to influence the work reported in this paper.

Acknowledgments

This work was supported by the Major Research Plan of the National Natural Science Foundation of China (No. 92472116), and the Central South University Innovation-Driven Research Program (No. 2023CXQD038).

Supplementary materials

Supplementary material associated with this article can be found, in the online version, at doi:10.1016/j.cclet.2025.111388.

References

[1] L. Tang, H. Peng, J. Kang, et al., Chem. Soc. Rev. 53 (2024) 4877–4925.
[2] Z. Liu, L. Qin, X. Cao, et al., Prog. Mater Sci. 125 (2022) 100911.
[3] S.W.D. Gourley, R. Brown, B.D. Adams, et al., Joule 7 (2023) 1415–1436.
[4] Y. Hu, P. Wang, M. Li, et al., Energ. Environ. Sci. 17 (2024) 8078–8093.
[5] J. Xu, H. Li, Y. Jin, et al., Adv. Mater. 36 (2023) 2309726.
[6] Z. Cai, J. Wang, Y. Sun, eScience 3 (2023) 100093.
[7] J. Chen, S. Li, F. Li, et al., ACS Appl. Mater. Inter. 16 (2024) 42153–42163.
[8] Y. Song, M. Chen, Z. Zhong, et al., Nat. Commun. 16 (2025) 3142.
[9] Z. Liu, L. Li, L. Qin, et al., Adv. Mater. 34 (2022) e2204681.
[10] Y. Kim, Y. Park, M. Kim, et al., Nat. Commun. 13 (2022) 2371.
[11] X. Dou, X. Xie, S. Liang, et al., Sci. Bull. 69 (2024) 833–845.
[12] W. Yang, Y. Yang, H. Yang, et al., ACS Energy Lett. 7 (2022) 2515–2530.
[13] D. Sheng, X. Liu, Z. Yang, et al., Adv. Funct. Mater. 34 (2024) 2402014.
[14] X. Guo, J. Lu, M. Wang, et al., Chem 10 (2024) 3607–3621.
[15] X. Feng, P. Li, J. Yin, et al., ACS Energy Lett. 8 (2023) 1192–1200.
[16] J. Zhou, Q. Li, X. Hu, et al., Chin. Chem. Lett. 35 (2024) 109143.
[17] W. Chen, Y. Wang, F. Wang, et al., Adv. Mater. 36 (2024) 2411802.
[18] Y. Wang, X. Lin, L. Wang, et al., Adv. Funct. Mater. 33 (2023) 2211088.
[19] H. Yan, S. Li, Y. Nan, et al., Adv. Energy Mater. 11 (2021) 2100186.
[20] L. Hong, X. Wu, C. Ma, et al., J. Mater. Chem. A 9 (2021) 16814–16823.
[21] H. Xu, R. Zhang, D. Luo, et al., ACS Nano 17 (2023) 25291–25300.
[22] Y. Wang, Y. Fan, D. Liao, et al., Energy Storage Mater. 51 (2022) 212–222.
[23] Z. Liu, M. Qin, B. Fu, et al., Angew. Chem. Int. Ed. 64 (2025) e202417049.
[24] D. Tang, X. Zhang, D. Han, et al., Adv. Mater. 36 (2024) e2406071.
[25] R. Deng, Z. He, F. Chu, et al., Nat. Commun. 14 (2023) 4981.
[26] R. Deng, J. Chen, F. Chu, et al., Adv. Mater. 36 (2024) 2311153.
[27] F. Li, C. Zhou, J. Zhang, et al., Adv. Mater. 36 (2024) 2408213.
[28] J. Zheng, G. Zhu, X. Liu, et al., ACS Energy Lett. 7 (2022) 4443–4450.
[29] H.M. Zhou, X.C. Qiao, J.G. Yu, Appl. Clay Sci. 80-81 (2013) 176–181.
[30] G. Qu, K. Guo, W. Chen, et al., Energ. Environ. Mater. 6 (2023) e12502.
[31] H. Cao, X. Zhang, B. Xie, et al., Adv. Funct. Mater. 33 (2023) 2305683.
[32] S. Zhang, H. Mei, B. Li, et al., Chin. Chem. Lett. 37 (2026) 111174.
[33] X. Xu, X. Feng, M. Li, et al., Chem. Eng. J. 478 (2023) 147313.
[34] X. Wu, Y. Xia, S. Chen, et al., Small 20 (2024) e2306739.
[35] I. Aguilar, J. Brown, L. Godeffroy, et al., Joule 9 (2024) 101784.
[36] M. Tian, C. Zhu, K. Luo, Chin. Chem. Lett. 37 (2026) 110702.
[37] Z. Feng, Y. Zhang, Z. Gao, et al., Adv. Powder Mater. 3 (2024) 100167.
[38] Y. Pan, Z. Liu, S. Liu, et al., Adv. Energy Mater. 13 (2023) 2203766.
[39] X. Xu, X. Feng, M. Li, et al., Small 20 (2024) e2308273.